TheoreticalModelling Of Infrared Photodetector for CO_2 Gas Detection

Trilok Kumar Parashar
University Polytechnic, Birla Institute of Technology, MESRA, Ranchi,

ABSTRACT
Numerical computation has been carried out for theoretical characterization of a p^+-InSb/n^0-InSb/n^+-InSb photodiode at 300 K for operation in 4.0 µm to 4.5 µm wavelength region. The different components of the dark current and the R_0A products have been calculated using the theoretical model discussed above. In present work the the R_0A product as well as the other major parameters of the p^+-InSb/n^0-InSb/n^+-InSbgas detectors such as quantum efficiency, responsivity and detectivity have been estimated quantitatively. The peak detectivity has been estimated to be ~ 6.8×10^7 mHz$^{1/2}$/W and efficiency obtained on the basis of this model with their peaks at 4.2 µm wavelength, which reveals that this detector is best suited for detection of CO_2 gas.

Index Terms
Detectivity, Responsivity, Efficiency, Gas detector

1. INTRODUCTION
The presence of any toxic gas and its amount needs to be monitor for different applications such as safety alarm for toxic gases in mines, CO and CO_2 monitoring in car exast, environmental monitoring etc. Every material and gas has a unique fundamental fingerprint in terms of their characteristic absorption band. An emission spectrum of a particular gas and its intensity measurement quantifies the amount of gas present at a particular space. A number of pollutant combustible/toxic gases and liquids such as hydrocarbons like NH_3 (2.3 µm), H_2S (2.7 µm), CH_4

(3.3 µm), CO_2(4.2 µm), CO (4.6) etc having their characteristic absorption band located in the infrared IR region. So a photodetector can be modeled for obtaining best performance about characteristic wavelengths of a particular gas and are best suited for

monitoring that gas. Several photodetector models are proposed by several researchers [1]-[10] for monitoring various toxic gases

2. Modelling of CO_2 gas detector: Structure and Formulation of model
The structure under consideration is p^+-InSb/ n^0-InSb/n^+-InSb photo-diode grown on a GaAs substrate as shown in Fig. 1. The top p^+ layer receives the incident light and the lightly doped n^0 region acts as the active layer.The incident light is absorbed in the neutral p^+, n^0 regions as well as in the space charge region formed at the p^+-n^0 junction. The carriers generated in the neutral p^+ and n^0 regions beyond their respective diffusion lengths will recombine before reaching the junction and fail to contribute to the net photocurrent.

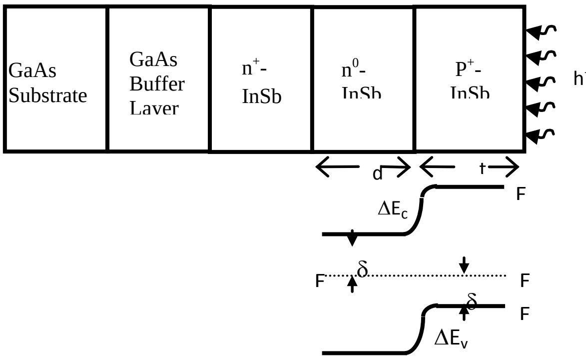

Fig. 1Schematic diagram of the gas detector

2.1 DARK CURRENT
The dark current of the InSb photodetector has been modeled here by considering the components arising from diffusion, generation-recombination and tunneling of carriers.

(i) Current due to diffusion of the thermally generated carriers from the neutral regions, I_{Diff}

(ii) Current due to generation-recombination of carriers in the depletion region, I_{GR}

(iii) The current resulting from tunneling of carriers through the barrier, I_{TUN}, which constitutes two components: I_{TAT} arising from the trap assisted tunneling and I_{BTB} arises out of band-to-band tunneling.

$$I_{TUN} = I_{TAT} + I_{BTB} \qquad [1]$$

The total dark current can be written as

$$\mathrm{I_{Total} = I_{Diff} + I_{GR} + I_{Tun}} \qquad [2]$$

In the analysis, all the three dominant recombination processes e.g., Auger, Radiative and Shockley-Read-Hall (SRH) recombination mechanisms are taken in account for computation of minority carrier lifetime. The mean lifetime of the carriers due to Auger recombination has been estimated on the basis of the three most dominant mechanisms e.g., Auger-1 (CHCC), Auger-7 (CHLH) and Auger-S (CHSH) transitions.

2.2 Effective Lifetime
The effective lifetime of the carriers has been obtained as

$$\frac{1}{\tau_{eff}} = \frac{1}{\tau_{AU}} + \frac{1}{\tau_{RAD}} + \frac{1}{\tau_{SRH}} \qquad [3]$$

The detailed expressions of the life times of photodetectors are discussed from references[4],[7] and [10].

The net or the effective value of zero bias resistance area product $(R_0A)_{Net}$ is given by

$$\frac{1}{(R_0A)_{Net}} = \frac{1}{(R_0A)_{Diff}} + \frac{1}{(R_0A)_{GR}} + \frac{1}{(R_0A)_{Tun}} \quad [4]$$

2.3 Quantum Efficiency And Specific Detectivity:

The quantum efficiency (η) of a p–n junction photodetector has generally three major components. These components arise from the contribution of the three regions e.g., neutral n-region (η_n), neutral p-region (η_p) and the depletion region (η_{dep}). The net quantum efficiency can be obtained by

$$\eta = \eta_n + \eta_p + \eta_{dep} \quad [5]$$

The quantum efficiency components contributed by the neutral n^0 and p^+ regions can be obtained finally as [4],[7]

$$\eta_p = \frac{(1-r_p)\alpha_p L_n}{\alpha_p^2 L_n^2 - 1} \left[\frac{\alpha_p L_n + \gamma_n - \exp\{-\alpha_p(t-x_p)\}\left[\gamma_n \cosh\left(\frac{t-x_p}{L_n}\right) + \sinh\left(\frac{t-x_p}{L_n}\right)\right]}{\gamma_n \sinh\left(\frac{t-x_p}{L_n}\right) + \cosh\left(\frac{t-x_p}{L_n}\right)} - \alpha_p L_n \exp\{-\alpha_p(t-x_p)\} \right]$$

[6]

$$\eta_n = \frac{(1-r_p)(1-r_n)\,\alpha_n L_p}{\alpha_n^2 L_p^2 - 1} \exp\{-(\alpha_p t + \alpha_n w_n)\} \left[\frac{(\gamma_p - \alpha_n L_p)\exp\{-\alpha_n(d-x_n)\} - \left[\gamma_p \cosh\left(\frac{d-x_n}{L_p}\right) + \sinh\left(\frac{d-x_n}{L_p}\right)\right]}{\gamma_p \sinh\left(\frac{d-x_n}{L_p}\right) + \cosh\left(\frac{d-x_n}{L_p}\right)} + \alpha_n L_p \right]$$

[7]

where $\gamma_n = \frac{S_n L_n}{D_n}$ and $\gamma_p = \frac{S_p L_p}{D_p}$

The quantum efficiency due to the contribution of the photo-generated carriers in the depletion region can be obtained as

$$\eta_{dep} = (1-r_n)(1-r_p)\left[\exp(-\alpha_p(t-x_p)) - \exp(-(\alpha_p t + \alpha_n x_n))\right] \quad [8]$$

2.4 RESPONSIVITY

The photoresponsivityis

$$\Re = \frac{q\eta\lambda}{hc} \quad [9]$$

Where, η is the quantum efficiency λ is the operating wavelength

2.5 SPECIFIC DETECTIVITY

The specific detectivity of the photodetector under consideration can be written as

$$D^* = \frac{q\eta\lambda}{hc}\sqrt{\frac{(R_0A)_{NET}}{4kT}} \quad [10]$$

where, η is the quantum efficiency, λ is the operating wavelength and $(R_0A)_{NET}$ is the net or effective value of the zero-bias resistance area product arising out of various components (e.g. diffusion, generation-recombination and tunneling) from references[7] ,[10]

3. RESULTS AND DISCUSSION

Numerical computation has been carried out for theoretical characterization of a p^+-InSb/n^0-InSb/n^+-InSb photodiode at 300 K for operation in 4.0 μm to 4.5 μm wavelength region. The parameters used for computation are taken from ref [1] , [6].

The different components of the dark current and the R_0A products have been calculated using the theoretical model discussed above. In present work the the R_0A product as well as the other major parameters of the p^+-InSb/n^0-InSb/n^+-InSbgas detectors such as quantum efficiency, responsivity and detectivity have been estimated quantitatively. Various other parameters used in the theoretical computations are taken from references [7]-[9]

Fig. 2 shows the current-voltage characteristics of the detector in the dark condition.

.

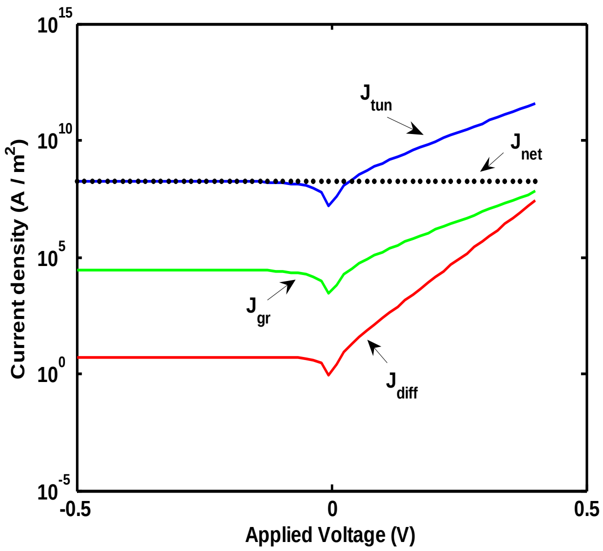

Fig. 2 Variation of the net dark current & its component with applied voltage

The components constituting darkcurrent e.g. diffusion, generation-recombination and tunneling (including the combined effect of trap-assisted and band-to-band components) and their variations with the applied voltage are also shown in the figure.

It is seen that the tunneling component of current density dominates over the net current density. Computations also reveal that the generation-recombination component also slightly affected net current density in forward bias.

In Fig. 3, the variation of net zero bias area product (R_0A_{net}) and its componentsis shown with applied voltage.

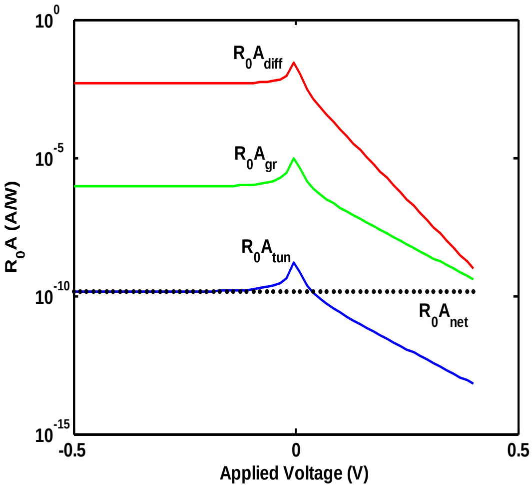

Fig. 3 Variation of R_0A_{net} and itscomponents with applied voltage

As obvious, the R_0A_{net} value depends on the tunneling component of zero bias area product, it is slightly affected by generation-recombination component and it is not affected by diffusion component.

Actual nature of the I-V characteristic of the detector is largely dependent on the processing history of the device.

Fig.4 shows the quantum efficiency of the detector with respect to operating wavelength. Here efficiency having its maximum value ≈ 0.45 at wavelength 4.2 µm and decreases sharply on the both side. So the device operates well between the wavelength ranges 4.1 µm to 4.4 µm.

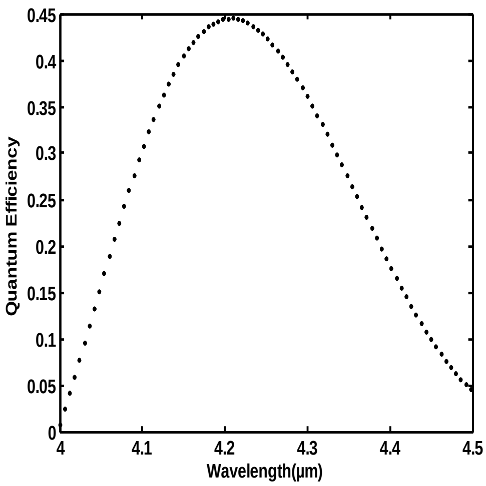

Fig. 4 Variation of the efficiency with operating wavelength

In Fig. 5, the variation of the responsivity of the gas detector with operating wavelength ranges 4.1µm to 4.30 µm, its maximum value 2.8 (A/W) at the wavelength 4.2 µm and decreases sharply on the both side.

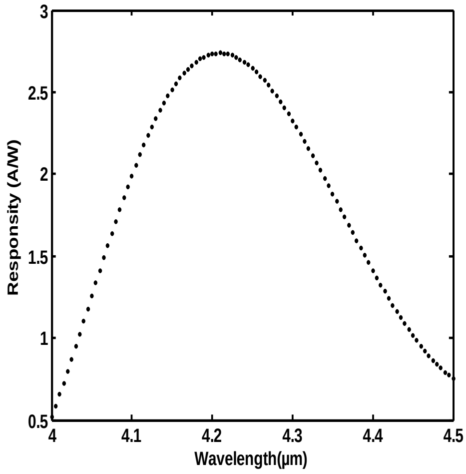

Fig. 5 Variation of the responsivity withoperating wavelength

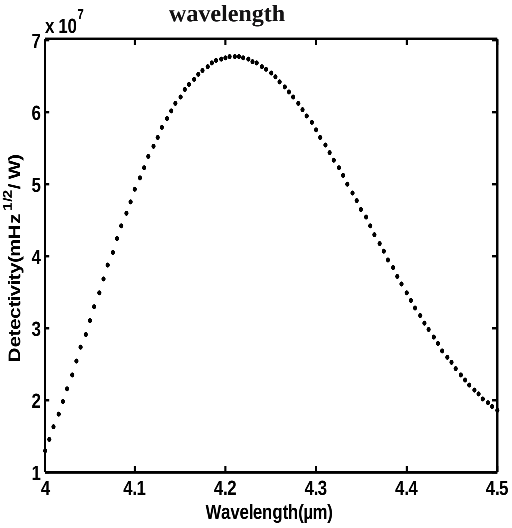

Fig. 6 Variation of the detectivitywith operating wavelength

The detectivity falls rapidly near the long wavelength cutoff. The peak detectivity has been estimated to be ~ 6.8 × 10^7 mHz$^{1/2}$/W at the wavelength λ = 4.2 µm.

Fig. 6 depicts the variation of the detectivity of the device with the wavelength of operation. It is seen that detectivity of the device at room temperature increases with increase in wavelength which reaches a peak value at λ = 4.2 µm.

4. CONCLUSION

In this paper a generic model of a infrared photodetector has been carried out for theoretical characterization of a p^+-InSb/n^0-InSb/n^+-InSb photodiode at 300 K for operation in 4.0 µm to 4.5 µm wavelength region. The model has been applied to characterise theoretically an InSb homojunction photodetectorsuch as quantum efficiency, responsivity and detectivity have been estimatedfor peration at 4.2 µm.The peak detectivity has been estimated to be ~ 6.8 × 10^7

$mHz^{1/2}/W$ and efficiency obtained on the basis of this model with their peaks at 4.2 µm wavelength , which reveals that this detector is best suited for detection of gases such as CO_2.

Using the same modelelling procedure and considering the charecteristic wavelength of the selected gas one can be develop model for other toxic gas monitoring. Such model would reduce the experimental cost and time of developing the gas detector for toxic gas sensors.Also II-VI materials such as HgCdTe can also be selected for some toxic gas detectors for LWIR region.

5. REFERENCES

[1]. Gao,H.H. KrierA., SherstnevV.V.,2000.“Room temperature InAs0:89Sb0:11 photodetectors for CO detection at 4.6µm”, Appl. Phys. Lett. 77 pp. 872–874.

[2]. Rogalski, AdamiecK., and RutkowskiJ, 2000. “Narrow-Gap Semiconductor Photodiode”, (SPIE, Bellingham, USA.

[3]. Rogalski,1994. “New trends in semiconductor infrared detectors”, Opt. Eng. 33, 1395–1412.

[4]. ChakrabartiP., SaxenaP. K. &Lal R. K, 2006. “Analytical Simulation of an InAsSb photovoltaic Detector for Mid-Infrared Applications”, Int J Infrared Milli Waves, 27,1119-1132.

[5]. Ibrahim Kimukin, NecmiBiyikli and EkmelOzbay, 2003. “InSb high-speed photodetectors grown on GaAs substrate”, J. of Appl. Phy., No. 94, 8, pp 5414-5416,

[6]. Anderson, W. W.,. J. 1980.Infrared Phys. 20, 363.

[7]. ParasharT.K. and.Lal,R.K 2011. “Theoretical modelling of InP based photodetector for hydrogen fluoride gas detection in short wavelength region”, Optoelectronics And Advanced Materials – Rapid Communications Vol. 5, No. 7, pp. 732 – 737.

[8]. LevinshteinM., RumyantsevS., and Shur(Eds.): M. 1999. .Hand book series on Semiconductor Parameters, vol.1 and 2, World Scientific, London.

[9]. Rakovska, V. Berger, X. Marcadet, B. Vinter, K. Bouzehouane and Kaplan D., 2000. “Optical charecterization and room temperature life time measurements of high quality MBE-grown InAsS on Gasb”, Semiconductor Science and Technology, vol.15, pp.34-39.

[10]. .ParasharT.K and Lal R.K., 2011. “Modeling and Simulation of HgCdTe based photodetector for N_2O gas detection”, Journal of Electron Devices, Vol. 11, pp. 527-537.

[11]. http://webbook.nist.gov/chemistry

[12]. http://www.ioffe.rssi.ru/SVA/NSM.
.